Engineering Science and Technology, an International Journal 22 (2019) 1087–1097

HOSTED BY

Contents lists available at ScienceDirect

Engineering Science and Technology, an International Journal

journal homepage: www.elsevier.com/locate/jestch

Full Length Article

Nonlinear PID controller design for a 6-DOF UAV quadrotor system

Aws Abdulsalam Najm, Ibraheem Kasim Ibraheem *

University of Baghdad – College of Engineering, Electrical Engineering Department, 10001 Baghdad, Iraq

ARTICLE INFO

Article history:
Received 29 September 2018
Revised 17 January 2019
Accepted 17 February 2019
Available online 8 March 2019

Keywords:
UAV
Quadrotor
Nonlinear PID controller
Stability analysis
Motion control
Disturbance
Circular trajectory

ABSTRACT

A Nonlinear PID (NLPID) controller is proposed to stabilize the translational and rotational motion of a 6-Degree of Freedom (DOF) unmanned aerial vehicles (UAV) quadrotor system and enforce it to track a given trajectory with minimum energy and error. The complete nonlinear model of the 6-DOF quadrotor system is obtained using Euler-Newton formalism and used in the design process, taking into account the velocity and acceleration vectors resulting in a more accurate 6-DOF quadrotor model and closer to the actual system. Six NLPID controllers are designed, each for Roll, Pitch, Yaw, Altitude, and the Position subsystems, where their parameters are tuned using Genetic Algorithm (GA) to minimize a multi-objective Output Performance Index (OPI). The stability of the 6-DOF UAV subsystems has been analyzed in the sense of Hurwitz stability theorem under certain conditions on the gains of the NLPID controllers. The simulations have been accomplished under MATLAB/SIMULINK environment and included three different trajectories, i.e., circular, helical, and square. The proposed NLPID controller for each of the six subsystems of the 6-DOF UAV quadrotor system has been compared with the Linear PID (LPID) one and the simulations showed the effectiveness of the proposed NLPID controller in terms of speed, control energy, and steady-state error.

1. Introduction

A fully autonomous quadrotor is one of the UAVs where it does not need a pilot to be controlled. Quadrotor has four arms each one has a rotor on it. Two of the rotors placed on opposite arms rotate in a clockwise direction while the others rotate in a counter-clockwise direction. The quadrotor is an under-actuated system because the number of rotors is less than the number of DOF, this makes designing a controller is a difficult problem. Quadrotors applications have been increased in the last years because of their simple implementation, low cost, different sizes, and maneuverability. Many applications founded for danger places, disasters, and rescue [1–3], quadrotor applications in agriculture [4,5], and even in helpful jobs like [6,7]. The work in [8] is a good survey for quadrotor applications for entertainment. Many studies could be found for the multi-agent system and formation control like [9–11], and for more applications in multi-agent systems, we recommend [12]. Many researchers studied control design and development with different types of controllers. One of the most used controllers is the LPID control because of its simplicity, ease of implementation and widely used in industries [13–16]. On the other hand, it has many disadvantages: 1) sometimes it gives a high control signal due to the fact of the windup, thus, overshooting and continuing to increase as the accumulated error is unwound (offset by errors in the other direction), 2) the differentiator leads to noise amplification. Our focus in this paper is on the NLPID controller which has received much attention from many researchers in the last two decade. A nonlinear fractional order PID (FOPID) has been proposed in [17] which is a combination of the proportional gain and fractions of the derivative and integral actions to increase the flexibility of the controller. While in [18] the hyperbolic nonlinearity have been combined with the (FOPID) to get more robust and effective NLPID controller. An adaptive Gaussian NLPID controller has been analyzed in [19], while the researchers in [20] have proposed a NLPID controller derived by a combination of PID structure and backstepping procedure. Other researchers worked on integrated the classical PID and the sliding mode control (SMC) [21]. Many of these NLPID controllers have been studied on the quadrotor system, where a nonlinear PI/PID controller has been proposed in [22] to control the motion of a quadrotor using NLPI controller for the horizontal motion and NLPID for the vertical motion and the orientation. A sliding-mode based NLPID controller is designed in [23] where the controller parameters are tuned to minimize a multi-objective function using GA, but a simplified quadrotor model was used in the simulations which give inaccurate results. While

* Corresponding author.
E-mail addresses: aws.najm@coeng.uobaghdad.edu.iq (A.A. Najm), ibraheemki@coeng.uobaghdad.edu.iq (I.K. Ibraheem).

https://doi.org/10.1016/j.jestch.2019.02.005
2215-0986/

this controller comprises a high order derivative term which results in noise amplification and inaccuracy while estimating the derivative. Other controllers used for quadrotors are: LQR-PID [24], geometric control [25], nonlinear model predictive control [26], L1 control [27], fuzzy control [28,29]. Further studies for control algorithms with quadrotor systems can be found in [30].

A new NLPID controller modified from the one proposed in our previous work [31] is presented in this paper. The modification is achieved by adding a lower limit to the integrator term to increase the stability of the closed-loop system. Moreover, the 6-DOF quadrotor system stability verified using Hurwitz stability criterion and its performance is compared with the most widely used controller in process industries specially quadrotor systems, i.e., the LPID controller due to its simplicity, ease of implementation and wide applicability. The control system for the 6-DOF UAV consists of six NLPID controllers, three NLPID controllers for the translational system and the rest ones for the rotational system of the underlying UAV. Each NLPID controller has twelve tuning parameters; they are tuned using GA and optimized toward the minimization of the proposed multi-objective OPI, which is a weighted sum of the Integrated Time Absolute Error (ITAE) and the square of the control signal (USQR).

The structure of this paper is as follows: Section 2 presents the modeling of the 6-DOF quadrotor system. Next, Section 3 describes the problem statement. The main results: the NLPID controller design and stability analysis are given in Section 4. Section 5 illustrates the numerical simulations and discussions followed by a conclusion and future work in Section 6.

2. Mathematical modelling of the 6-DOF UAV quadrotor

To control any system, firstly, a mathematical model must be derived. This mathematical model will describe the responses of the system for different inputs. The inputs for the 6-DOF quadrotor system are combinations of the rotors speed (Ω), which in this case is a force f_t to control the altitude (z) and the torques (τ_x, τ_y, and τ_z) to control the angels (ϕ, θ, and ψ) respectively, see (1). The meaning of each parameter is described in Table 1.

$$\begin{cases} f_t = b\left(\Omega_1^2+\Omega_2^2+\Omega_3^2+\Omega_4^2\right) \\ \tau_x = bl\left(\Omega_3^2-\Omega_1^2\right) \\ \tau_y = bl\left(\Omega_4^2-\Omega_2^2\right) \\ \tau_z = d\left(\Omega_2^2+\Omega_4^2-\Omega_1^2-\Omega_3^2\right) \end{cases} \tag{1}$$

Table 1
Parameters Description.

Parameters	Description	Units
$[x\ y\ z]$	Linear position vector	m
$[\phi\ \theta\ \psi]$	Angular position vector	rad
$[u\ v\ w]$	Linear velocity vector	m/s
$[p\ q\ r]$	Angular velocity vector	rad/s
$[I_x\ I_y\ I_z]$	Moment of inertia vector	kg.m^2
f_t	Total thrust generated by rotors	N
$[\tau_x\ \tau_y\ \tau_z]$	Control torques	N.m
$[f_{wx}\ f_{wy}\ f_{wz}]$	Wind force vector	N
$[\tau_{wx}\ \tau_{wy}\ \tau_{wz}]$	Wind torque vector	N.m
g	Gravitational force	m/s^2
m	Total mass	kg
$[\Omega_1\ \Omega_2\ \Omega_3\ \Omega_4]$	Rotors speeds vector	rad/s
b	Thrust coefficient	N.s^2
l	Motor to center length	m
d	Drag coefficient	N.m.s^2

$c() \equiv cos(), s() \equiv sin(), and\, t() \equiv tan()$

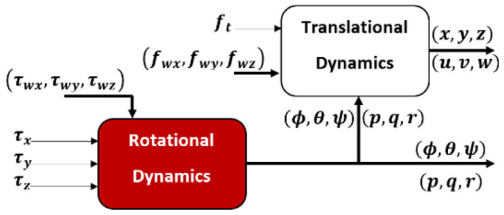

Fig. 1. 6-DOF Quadrotor system Dynamics Relations.

Some researchers [13–15,32] depend only on the equations of acceleration for the 6-DOF quadrotor system without taking the velocities into account. In this paper, the mathematical model of the 6-DOF quadrotor system is crafted in such a way that the acceleration and velocity vectors are taken into consideration resulting in a more accurate nonlinear model for the 6-DOF quadrotor system and closer to the actual one. The equations of the nonlinear mathematical model of the 6-DOF quadrotor system are derived based on Euler-Newton formaliation to represent the 3D motion of the rigid body and written in (2) [33,34]. Fig. 1 shows the block diagram of the 6-DOF quadrotor dynamical relations.

$$\begin{cases} \begin{pmatrix}\dot{x}\\ \dot{y}\\ \dot{z}\end{pmatrix} = \begin{pmatrix} c(\psi)c(\theta) & [c(\psi)s(\phi)s(\theta)-c(\phi)s(\psi)] & [s(\phi)s(\psi)+c(\phi)c(\psi)s(\theta)] \\ c(\theta)s(\psi) & [c(\phi)c(\psi)+s(\phi)s(\psi)s(\theta)] & [c(\phi)s(\psi)s(\theta)-c(\psi)s(\phi)] \\ -s(\theta) & c(\theta)s(\phi) & c(\phi)c(\theta)) \end{pmatrix} \begin{pmatrix}u\\ v\\ w\end{pmatrix} \\ \begin{pmatrix}\dot{u}\\ \dot{v}\\ \dot{w}\end{pmatrix} = \begin{pmatrix} 0 & r & -q \\ -r & 0 & p \\ q & -p & 0 \end{pmatrix} \begin{pmatrix}u\\ v\\ w\end{pmatrix} + g\begin{pmatrix} -s(\theta) \\ s(\phi)c(\theta) \\ c(\phi)c(\theta) \end{pmatrix} + \frac{1}{m}\begin{pmatrix} f_{wx} \\ f_{wy} \\ f_{wz}-f_t \end{pmatrix} \\ \begin{pmatrix}\dot{\phi}\\ \dot{\theta}\\ \dot{\psi}\end{pmatrix} = \begin{pmatrix} 1 & s(\phi)t(\theta) & c(\phi)t(\theta) \\ 0 & c(\phi) & -s(\phi) \\ 0 & \frac{s(\phi)}{c(\theta)} & \frac{c(\phi)}{c(\theta)} \end{pmatrix} \begin{pmatrix}p\\ q\\ r\end{pmatrix} \\ \begin{pmatrix}\dot{p}\\ \dot{q}\\ \dot{r}\end{pmatrix} = \begin{pmatrix} \frac{I_y-I_z}{I_x} \\ \frac{I_z-I_x}{I_y} \\ \frac{I_x-I_y}{I_z} \end{pmatrix} \begin{pmatrix} rq \\ pr \\ pq \end{pmatrix} + \begin{pmatrix} \frac{\tau_x+\tau_{wx}}{I_x} \\ \frac{\tau_y+\tau_{wy}}{I_y} \\ \frac{\tau_z+\tau_{wz}}{I_z} \end{pmatrix} \end{cases} \tag{2}$$

To control the 6-DOF quadrotor system, a combination of translational (x, y, z) and rotational (ϕ, θ, ψ) motions is needed. From Newton's law [33]:

$$\begin{pmatrix}\ddot{x}\\ \ddot{y}\\ \ddot{z}\end{pmatrix} = -\frac{f_t}{m}\begin{pmatrix} s(\phi)s(\psi)+c(\phi)c(\psi)s(\theta) \\ c(\phi)s(\psi)s(\theta)-c(\psi)s(\phi) \\ c(\phi)c(\theta) \end{pmatrix} + \begin{pmatrix}0\\ 0\\ g\end{pmatrix} \tag{3}$$

3. Problem statement

Suppose that the equations below represent the nonlinear 6-DOF quadrotor system shown in Fig. 2:

$$\begin{cases} X^n = F\left(X, \dot{X}, \ldots, X^{n-2}, X^{n-1}\right) + G(X)U \\ Y = X \end{cases} \tag{4}$$

where $X = Y = [x, y, z, \phi, \theta, \psi, u, v, w, p, q, r] \in \mathbb{R}^{12}$ is the linear, angular position and velocity vectors of the quadrotor system, where Y is the measured output, $U = \left[U_x, U_y, U_z, U_\phi, U_\theta, U_\psi\right] \in \mathbb{R}^6$ is the control input vector of the 6-DOF quadrotor system which needs to be designed such that it stabilizes the underactuated unstable 6-DOF quadrotor system and makes it follows a specific trajectory subject to optimum time-domain specifications and minimum control energy.

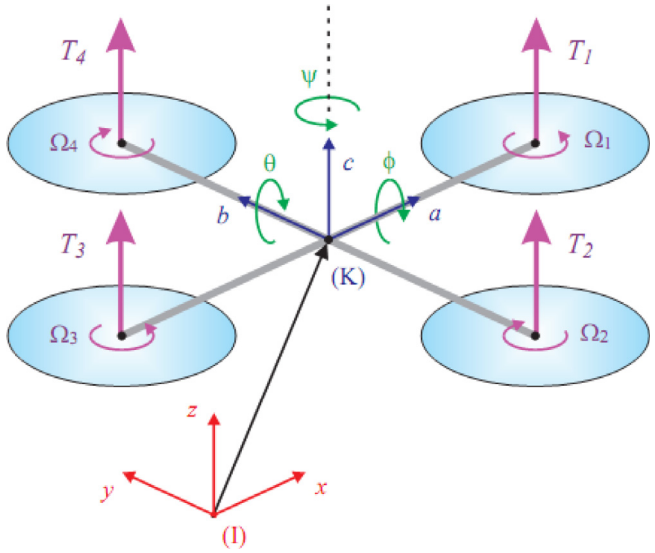

Fig. 2. 6-DOF quadrotor System.

4. Main results

4.1. Nonlinear controller design

Given the LPID controller,

$$U_{PID} = K_p e + K_d \dot{e} + K_i \int e\,dt \tag{5}$$

which is a linear combination of the error signal $e \in \mathbb{R}$, its derivative $\dot{e} \in \mathbb{R}$, and its integral $\int e\,dt \in \mathbb{R}$ weighted by the gains $(K_p, K_d, K_i) \in \mathbb{R}^+$ respectively. The NLPID controller has been developed to get a more satisfactory response for the nonlinear 6-DOF quadrotor system, where it replaces each term of the LPID controller with a nonlinear function $f(e)$ which is a nonlinear combination of sign and exponential functions of the error signal, its derivative and its integral as given below

$$\begin{cases} U_{NLPID} = f_1(e) + f_2(\dot{e}) + f_3\left(\int e\,dt\right) \\ f_i(\beta) = k_i(\beta)|\beta|^{\alpha_i} sign(\beta) \\ k_i(\beta) = k_{i1} + \frac{k_{i2}}{1+exp\left(\mu_i \beta^2\right)}, i = 1,2,3 \end{cases} \tag{6}$$

where β could be e, $\dot{e}$, or $\int e\,dt, \alpha_i \in \mathbb{R}^+$, the function $k_i(\beta)$ is a positive function with coefficients $k_{i1}, k_{i2}, \mu_i \in \mathbb{R}^+$. In order to increase the sensitivity of the NLPID controller for small errors, the nonlinear gain term $k_i(\beta)$ is used. For small errors close to zero, the value of the nonlinear gain term $k_i(\beta)$ approaches the upper bound $k_{i1} + k_{i2}/2$. While for large errors, the nonlinear gain term $k_i(\beta)$ approaches the lower bound k_{i1}, which means that the nonlinear gain term $k_i(\beta)$ is bounded in the sector $[k_{i1}, k_{i1} + k_{i2}/2]$, see Fig. 3. Less control energy is obtained with the NLPID control while the error is changing continuously. In this paper the NLPID controller is designed as in [31] with modification in the integral term of (6), where a lower limit k_{31} is added to the integral term.

Because of the underactuated phenomenon of the 6-DOF quadrotor system, the control system for the 6-DOF quadrotor system is divided into two parts. The First part is where the input control is available, it is called the *Inner-Loop Control(ILC)*, while the second part is where there is no actual input control available and it is called the *Outer-Loop Control(OLC)*.

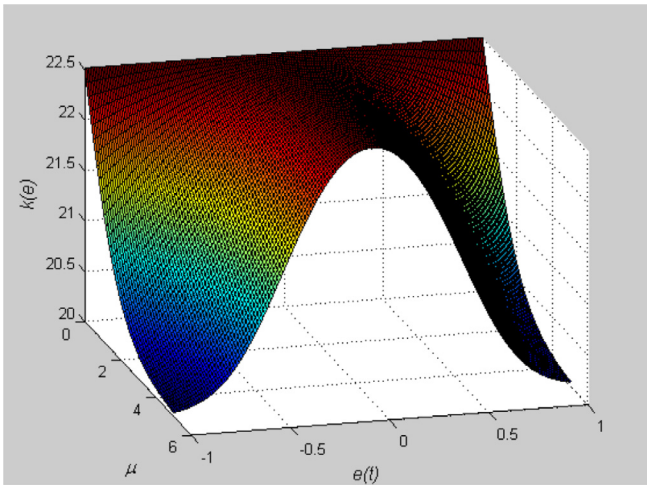

Fig. 3. Characteristics of the nonlinear gain function $k(e)$ for i = 1, $k_{11} = 20, k_{12} = 5$ [31].

4.1.1. Nonlinear design for ILC

The proposed control signals for the altitude z and the attitude (ϕ, θ, and ψ) motions are given as follows.

The throttle force control f_t is given as

$$\begin{aligned} U_z &= f_t = f_{z1}(e_z) + f_{z2}(\dot{e}_z) + f_{z3}\left(\int e_z\,dt\right) \\ e_z &= z_{de} - z_{ac} \end{aligned} \tag{7}$$

While the Roll torque control signal τ_x is given as

$$\begin{aligned} U_\phi &= \tau_x = f_{\phi 1}(e_\phi) + f_{\phi 2}(\dot{e}_\phi) + f_{\phi 3}\left(\int e_\phi\,dt\right) \\ e_\phi &= \phi_{de} - \phi_{ac} \end{aligned} \tag{8}$$

The Pitch torque control signal τ_y is given as

$$\begin{aligned} U_\theta &= \tau_y = f_{\theta 1}(e_\theta) + f_{\theta 2}(\dot{e}_\theta) + f_{\theta 3}\left(\int e_\theta\,dt\right) \\ e_\theta &= \theta_{de} - \theta_{ac} \end{aligned} \tag{9}$$

Finally, the Yaw torque control τ_z can be designed as

$$\begin{aligned} U_\psi &= \tau_z = f_{\psi 1}(e_\psi) + f_{\psi 2}(\dot{e}_\psi) + f_{\psi 3}\left(\int e_\psi\,dt\right) \\ e_\psi &= \psi_{de} - \psi_{ac} \end{aligned} \tag{10}$$

where the subscript "*de*" means desired reference values, "*ac*" means the actual or measured values from different sensors of the 6-DOF quadrotor system, $(f_{zi}, f_{\phi i}, f_{\theta i}, f_{\psi i}), i = 1,2,3$ are the NLPID controller gains represented in (6).

4.1.2. Nonlinear design for OLC

Quadrotor system has no real control input for the motion in the (x,y) plane, the following analysis is proposed to generate the appropriate control signals (U_x and U_y) for the motion in the (x,y) plane, see (3). Simplifying the model of (3) by assuming the ϕ and θ angle deviations are small (i.e. β is small $\Rightarrow c(\beta) = 1, s(\beta) = \beta$).

$$\begin{pmatrix} \ddot{x} \\ \ddot{y} \end{pmatrix} = \frac{U_z}{m} \begin{pmatrix} -s(\psi) & -c(\psi) \\ c(\psi) & -s(\psi) \end{pmatrix} \begin{pmatrix} \phi_{de} \\ \theta_{de} \end{pmatrix} \tag{11}$$

$$\begin{pmatrix} \phi_{de} \\ \theta_{de} \end{pmatrix} = \frac{m}{U_z} \begin{pmatrix} -s(\psi) & -c(\psi) \\ c(\psi) & -s(\psi) \end{pmatrix}^{-1} \begin{pmatrix} \ddot{x} \\ \ddot{y} \end{pmatrix} \tag{12}$$

The main objective of the NLPID controller is to get the errors of x and y positions approach zero as described below

$$\begin{cases} \ddot{x}_{de} - \ddot{x}_{ac} + f_{x1}(e_x) + f_{x2}(\dot{e}_x) + f_{x3}\left(\int e_x\,dt\right) \\ \qquad = 0 \\ \ddot{y}_{de} - \ddot{y}_{ac} + f_{y1}(e_y) + f_{y2}(\dot{e}_y) + f_{y3}\left(\int e_y\,dt\right) \\ \qquad = 0 \end{cases} \tag{13}$$

Substitute $\ddot{x}_{ac}, \ddot{y}_{ac}$ of (13) into (12), yields,

$$\begin{pmatrix} \phi_{de} \\ \theta_{de} \end{pmatrix} = \frac{m}{U_z} \begin{pmatrix} -s(\psi) & -c(\psi) \\ c(\psi) & -s(\psi) \end{pmatrix}^{-1} \times \begin{pmatrix} \ddot{x}_{de} + f_{x1}(e_x) + f_{x2}(\dot{e}_x) + f_{x3}(\int e_x\, dt) \\ \ddot{y}_{de} + f_{y1}(e_y) + f_{y2}(\dot{e}_y) + f_{y3}(\int e_y\, dt) \end{pmatrix} \tag{14}$$

Letting U_x, U_y be the virtual control signals for x, y respectively, which are proposed as follows

$$\begin{aligned} U_x &= \ddot{x}_{ac} = f_{x1}(e_x) + f_{x2}(\dot{e}_x) + f_{x3}(\int e_x\, dt) + \ddot{x}_{de} \\ e_x &= x_{de} - x_{ac} \end{aligned} \tag{15}$$

$$\begin{aligned} U_y &= \ddot{y}_{ac} = f_{y1}(e_y) + f_{y2}(\dot{e}_y) + f_{y3}(\int e_y\, dt) + \ddot{y}_{de} \\ e_y &= y_{de} - y_{ac} \end{aligned} \tag{16}$$

where $(f_{xi}, f_{yi}), i = 1, 2, 3$ are the NLPID controller gains given in (6). Now, (14) can be written as,

$$\begin{pmatrix} \phi_{de} \\ \theta_{de} \end{pmatrix} = \frac{m}{U_z} \begin{pmatrix} -s(\psi) & c(\psi) \\ -c(\psi) & -s(\psi) \end{pmatrix} \begin{pmatrix} U_x \\ U_y \end{pmatrix} \tag{17}$$

The Overall controlled quadrotor system is shown in Fig. 4.

Remark 1. To investigate the stability of the 6-DOF quadrotor system based on its nonlinear model, the nonlinear model equations of (2) is converted into six subsystems each one can be represented by a second order Brunovsky form given as

$$\begin{cases} \dot{\zeta}_1 = \zeta_2 \\ \dot{\zeta}_2 = F_U + hU_\zeta \end{cases} \tag{18}$$

where $\zeta_1 = \{x, y, z, \phi, \theta, \psi\} \in \mathbb{R}, \zeta_2 = \{u, v, w, p, q, r\} \in \mathbb{R}, U_\zeta = \{U_x, U_y, -U_z, U_\phi, U_\theta, U_\psi\} \in \mathbb{R}$ and $h \in \mathbb{R}^+, F_U$ is an unknown function which needs to be identified to analyze the stability of (18). Some studies like [35,36] proposed an extended state observer to estimate the unknown function F_U, while [37] proposed a radial basis function (RBF) to approximate F_U and include it in the proposed control law. Since our proposed nonlinear PID controller belongs to a class of passive controllers, where the unknown function cannot be estimated by the controller itself, the stability test is based on the linearized model where the unknown function F_U is diminished.

4.2. Stability analysis of the closed-loop system

In this section, the overall stability analysis of both the ***ILC*** and ***OLC*** subsystems will be demonstrated using Routh-Hurwitz stability criterion on the linearized model of the 6-DOF quadrotor derived in [33] with the virtual controllers U_x and U_y proposed in (15) and (16) respectively. The linearized model of the overall 6-DOF quadrotor system is represented as

$$\left\{ \begin{aligned} \dot{x}_1 &= x_2 \\ \dot{x}_2 &= U_\phi / I_x \end{aligned} \right\} (19.a)$$
$$\left\{ \begin{aligned} \dot{x}_3 &= x_4 \\ \dot{x}_4 &= U_\theta / I_y \end{aligned} \right\} (19.b)$$
$$\left\{ \begin{aligned} \dot{x}_5 &= x_6 \\ \dot{x}_6 &= U_\psi / I_z \end{aligned} \right\} (19.c)$$
$$\left\{ \begin{aligned} \dot{x}_7 &= x_8 \\ \dot{x}_8 &= U_x \end{aligned} \right\} (19.d)$$
$$\left\{ \begin{aligned} \dot{x}_9 &= x_{10} \\ \dot{x}_{10} &= U_y \end{aligned} \right\} (19.e)$$
$$\left\{ \begin{aligned} \dot{x}_{11} &= x_{12} \\ \dot{x}_{12} &= -U_z / m \end{aligned} \right\} (19.f)$$

(19)

where $\mathbf{x} \in \mathbb{R}^{12} : \mathbf{x} = [\phi, p, \theta, q, \psi, r, x, u, y, v, z, w]$. Each one of the six subsystems described in (19) can be represented in the general form

$$\begin{cases} \dot{\eta}_1 = \eta_2 \\ \dot{\eta}_2 = hU_\eta \end{cases} \tag{20}$$

where $\eta_1, \eta_2 \in \mathbb{R}, \eta_1 = x_i, \eta_2 = x_{i+1}$ for $i = \{1, 3, 5, 7, 9, 11\}$, $U_\eta = \{U_\phi, U_\theta, U_\psi, U_x, U_y, -U_z\} \in \mathbb{R}$ and $h \in \mathbb{R}^+$. If the stability of system (20) is ensured then the 6-DOF quadrotor subsystems are stable and the overall quadrotor system is stable in the sense of Hurwitz stability theorem. Before proceeding, some assumptions are needed.

Assumption A1. In order to prove the stability of the quadrotor system (19), all α,s in (6) will be approximated to 1, since the tuned values of α,s for the six controllers were almost around one, i.e. $\alpha_i \approx 1, i = 1, 2, \ldots, 6$ (i.e. $|\beta| sign(\beta) = \beta$).

Assumption A2. All the states x, y, z, ϕ, θ and ψ of the 6-DOF UAV quadrotor system are observable states, i.e. there is no need for the state observer. In case of non observable states, one can design an state observer or an extended state observer as in [35,36].

Theorem 1. *Given the NLPID controller proposed in (7)–(10), (15) and (16) for (19), if assumptions A1 and A2 hold true, then the closed-loop system is Hurwitz stable for* $k_1(e_1) \in \left[k_{11}, k_{11} + \frac{k_{12}}{2}\right]$, $k_3(e_0) \in \left[k_{31}, k_{31} + \frac{k_{32}}{2}\right]$, *and* $k_2(e_2) \in \left[k_{21}, k_{21} + \frac{k_{22}}{2}\right]$.

Proof. To proceed the proof of Theorem 1, each of the six subsystems of (19) can be represented by (20), where the error dynamics for the closed-loop system can be written as

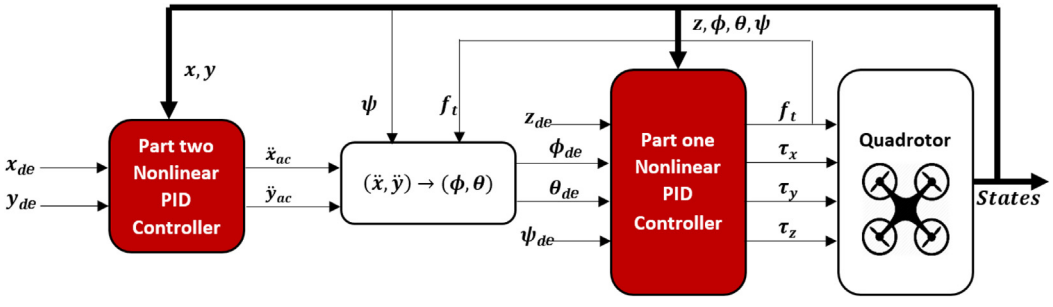

Fig. 4. Overall Quadrotor system.

$$\begin{cases} e_1 = \eta_{1_{de}} - \eta_{1_{ac}} \\ e_2 = \eta_{2_{de}} - \eta_{2_{ac}} \\ e_0 = \int e_1\, dt \end{cases} \tag{21}$$

Taking the derivative of (21) and knowing that $\dot{\eta}_{1_{de}} = \eta_{2_{de}}$ and $\dot{\eta}_{2_{de}} = 0$. This yields,

$$\begin{cases} \dot{e}_0 = e_1 \\ \dot{e}_1 = e_2 \\ \dot{e}_2 = -hU_\eta \end{cases} \tag{22}$$

Closing the loop by substituting the control signal (6) in (22) and expressing it in matrix form, we get,

$$\begin{bmatrix} \dot{e}_0 \\ \dot{e}_1 \\ \dot{e}_2 \end{bmatrix} = A_c \begin{bmatrix} e_0 \\ e_1 \\ e_2 \end{bmatrix} \tag{23}$$

where $A_c = \begin{bmatrix} 0 & 1 & 0 \\ 0 & 0 & 1 \\ -hk_3(e_0) & -hk_1(e_1) & -hk_2(e_2) \end{bmatrix}$

Finding the characteristics equation for A_c by the relation $|\lambda I - A_c| = 0$, yields,

$$\lambda^3 + hk_2(e_2)\lambda^2 + hk_1(e_1)\lambda + hk_3(e_0) = 0 \tag{24}$$

The Hurwitz Matrix for the characteristics equation is given as

$$H = \begin{bmatrix} hk_2(e_2) & hk_3(e_0) & 0 \\ 1 & hk_1(e_1) & 0 \\ 0 & hk_2(e_2) & hk_3(e_0) \end{bmatrix}$$

The conditions for the system (24) to be Hurwitz stable are given as

$\Delta_1 = hk_2(e_2) > 0$

$\Delta_2 = h^2k_1(e_1)k_2(e_2) - hk_3(e_0) > 0$

$\Delta_3 = h^3k_1(e_1)k_2(e_2)k_3(e_0) - h^2k_3^2(e_0) > 0$

$\Delta_3 = hk_3(e_0)\Delta_2 > 0$

As we stated before, $k_i(\beta)$ is sector bounded in the range $[k_{i1}, k_{i1} + k_{i2}/2]$ and always positive, assuming a range for any two of $\{k_1(e_1), k_2(e_2), k_3(e_0)\}$ will lead to the range of the third one, e.g., let $k_1(e_1) \in \left[k_{11}, k_{11} + \frac{k_{12}}{2}\right]$ and $k_3(e_0) \in \left[k_{31}, k_{31} + \frac{k_{32}}{2}\right]$, this will results in $k_2(e_2) > k_3(e_0)/hk_1(e_1)$ and gives $k_{21} > \frac{k_{31}}{hk_{11} + h\frac{k_{12}}{2}}$ and $k_{21} + \frac{k_{22}}{2} > \frac{k_{31} + \frac{k_{32}}{2}}{hk_{11}}$, which will ensure the closed-loop system to be stable in the sense of the Hurwitz stability theorem.

Remark 2. The linearized model (19) of the 6-DOF quadrotor is used only to prove the stability of the closed-loop quadrotor system, while the complete nonlinear model represented by (2) is used in the control design and simulations.

5. Simulation results and case studies

5.1. Step reference tracking

The 6-DOF nonlinear quadrotor dynamic model and the NLPID controller are implemented in MATLAB/Simulink, where we have assumed that the wind forces and torques $[f_{wx}, f_{wy}, f_{wz}, \tau_{wx}, \tau_{wy}, \tau_{wz}]$ are negligible. The parameters values of the quadrotor used in the simulations are listed in Table 2. In our simulations, an unconstrained multi-objective optimization is conducted to tune the parameters of the NLPID controllers, i.e.,

Find $\Gamma = [\Gamma_x, \Gamma_y, \Gamma_z, \Gamma_\phi, \Gamma_\theta, \Gamma_\psi]$ which minimizes

Table 2
Parameters Values.

Parameter	Value
I_x	8.5532×10^{-3}
I_y	8.5532×10^{-3}
I_z	1.476×10^{-2}
g	9.81×10^{0}
m	9.64×10^{-1}
b	7.66×10^{-5}
d	5.63×10^{-6}
l	2.2×10^{-1}

$$\begin{cases} opi_i = w_{1i} \times \frac{ITAE_i}{N_{1i}} + w_{2i} \times \frac{USQR_i}{N_{2i}} \\ OPI = \sum_i (\widehat{w}_i \times opi_i), i = x, y, z, \psi \end{cases} \tag{25}$$

where $\Gamma_\sigma = [k_{11}\ k_{12}\ k_{21}\ k_{22}\ k_{31}\ k_{32}\ \mu_1\ \mu_2\ \mu_3\ \alpha_1\ \alpha_2\ \alpha_3]$,
$\sigma = \{x, y, z, \phi, \theta, \psi\}$
while for the LPID controller
Find $\Gamma = [\Gamma_x, \Gamma_y, \Gamma_z, \Gamma_\phi, \Gamma_\theta, \Gamma_\psi]$ which minimizes (25) where $\Gamma_\sigma = [Kp\ Kd\ Ki], \sigma = \{x, y, z, \phi, \theta, \psi\}$.

The ITAE and USQR are defined in Table 3. The weighting variables must satisfy $w_{1i} + w_{2i} = 1$, They are defined as the relative emphasis of one objective as compared to the other. Their values are chosen to increase the pressure on the selected objective function. The same applies to the weighting variables $\widehat{w}_i$. While N_{1i} and N_{2i} are normalizing variables. They are included in the performance index to ensure that the individual objectives have comparable values, and are treated equally likely by the tuning algorithm. Because, if a certain objective is of very high value, while the second one has very low value, then the tuning algorithm will pay much consideration to the highest one and leave the other with little reflection on the system. The reason for taking just x, y, z, and ψ in the optimization process is due to the fact that the position of UAV is characterized by the 3D coordinates (x,y,z) and rotation about z-axis ψ. Adding ϕ and θ will result in a better performance but the optimization process will take longer time. The values of $w_{1i} = 0.6, w_{2i} = 0.4, \widehat{w}_i = 0.25, i = x, y, z, \psi; N_{1i} = N_{2i} = 1$ for $i = x, y, \psi$; while $N_{1z} = 1$ and $N_{2z} = 4500$. The values of both controllers after tuning are listed in Table 4 and Table 5. After tuning the overall quadrotor's six controllers, the performance indices for $(x, y, z,$ and $\psi)$ and the 6-DOF quadrotor total OPI are shown in Table 6.

Table 3
Performance Indices.

Performance Index	Description	Mathematical Representation
ITAE	Integrated time absolute error	$\int_0^{t_f} t\lvert e(t)\rvert\, dt$
USQR	Controller energy	$\int_0^{t_f} [u(t)]^2\, dt$

*t_f is the final time of simulation.

Table 4
LPID Parameters.

	k_p	k_i	k_d
x	2.8×10^{-1}	2.73×10^{-6}	6.3×10^{-1}
y	3.6×10^{-1}	1.56×10^{-5}	8.8×10^{-1}
z	1.8402×10^{2}	1.0373×10^{2}	2.25×10^{1}
ϕ	8.8×10^{-1}	9×10^{-1}	3×10^{-1}
θ	6.2×10^{-1}	8.1×10^{-1}	5×10^{-2}
ψ	9.9×10^{-1}	4.9×10^{-1}	5.6×10^{-1}

Table 5
NLPID Parameters.

	x	y	z	ϕ	θ	ψ
k_{11}	1.51×10^{0}	1.38×10^{0}	2.75×10^{1}	7.7×10^{-1}	4.8×10^{-1}	7.6×10^{-1}
k_{12}	4×10^{-2}	3×10^{-2}	8.76×10^{0}	6×10^{-2}	3×10^{-2}	1.6×10^{-1}
k_{21}	1.13×10^{0}	2.51×10^{0}	8.8×10^{0}	2×10^{-1}	8×10^{-2}	1.7×10^{-1}
k_{22}	1.8×10^{-1}	4×10^{-2}	4.71×10^{0}	4×10^{-2}	1.2×10^{-1}	1.1×10^{-1}
k_{31}	1.81×10^{-6}	5.72×10^{-5}	1.849×10^{1}	1.08×10^{0}	8.8×10^{-1}	2.7×10^{-1}
k_{32}	1×10^{-6}	8.69×10^{-6}	1.002×10^{1}	8×10^{-2}	1.1×10^{-1}	8×10^{-2}
μ_1	1.1×10^{-1}	8×10^{-2}	3.1×10^{-1}	7×10^{-2}	8.4×10^{-1}	2.5×10^{-1}
μ_2	8×10^{-2}	3.6×10^{-1}	3.6×10^{-1}	5.6×10^{-1}	1.43×10^{0}	4.6×10^{-1}
μ_3	1.8×10^{-1}	6×10^{-1}	9.8×10^{-1}	5.8×10^{-1}	2.8×10^{-1}	8.1×10^{-1}
α_1	9.3×10^{-1}	9.3×10^{-1}	9.6×10^{-1}	9.6×10^{-1}	9.6×10^{-1}	9.8×10^{-1}
α_2	9.3×10^{-1}	9.2×10^{-1}	9.7×10^{-1}	9.6×10^{-1}	1×10^{0}	9.5×10^{-1}
α_3	9.5×10^{-1}	9.3×10^{-1}	9.7×10^{-1}	9.7×10^{-1}	9.7×10^{-1}	9.2×10^{-1}

Table 6
Position and Yaw Performance indices.

	LPID		NLPID	
	ITAE	ISU	ITAE	ISU
x	14.285931	0.134411	0.438883	0.381936
y	7.498694	0.323482	1.066173	1.226223
z	0.059225	5197.496	0.152148	4516.303
ψ	1.377493	0.030779	0.506028	0.037517
OPI	3.6476		0.5894	

A unit step reference inputs (x_{de}, y_{de}, z_{de}, and ψ_{de}) have been applied to the position (x, y, and z) of the 6-DOF and the yaw (ψ) orientation. The curves in Fig. 5 (a), represent the response of the x-position of the quadrotor system using both controllers, while (b) represent the energy signal produced by the controllers to achieve the required position. The output response for y, z, and ψ are shown in Figs. 6–8. As can be seen, the control signal produced by the NLPID controller is less fluctuating than that of the LPID controller. The NLPID controller shows a faster response than the LPID one, except for the z-position, where the LPID controller presents a faster tracking, but on account of large control energy being spent. This increase in the energy of the control signal is undesired in the practice since it leads to actuator saturation. The overshoot in the output response for the PID controller is very clear. The output responses of ϕ and θ are drawn in Figs. 9 and 10 respectively which show the effectiveness of the proposed NLPID controller over the linear one.

This has been reflected in the energy of the control signal and the smoothness of the output response. Comparing the energy signals for ϕ and θ using both controllers, the NLPID controller presented a huge reduction as compared to the linear one. The time-domain specifications of both controllers are presented numerically in Table 7 (rising t_r, settling t_s and peak overshoot M_p) for the position (x, y, and z) of the quadrotor system and yaw(ψ) using both controllers. Table 8 shows the minimum and maximum peaks for ϕ and θ using both controllers. The difference between the responses of (ϕ, θ) and (x, y, z, ψ) which is very clear in Table 7 and Table 8 came from the fact that ϕ_d and θ_d are internally generated without external desired signal. While the signals (x_d, y_d, z_d and ψ_d) are the trajectory references that follow an external reference signals.

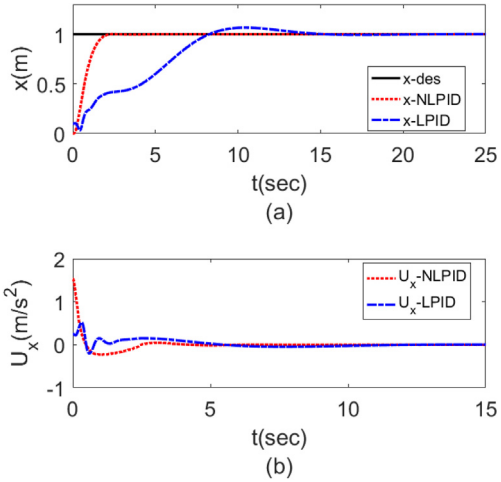

Fig. 5. x-Position (a) time response (b) controller signal.

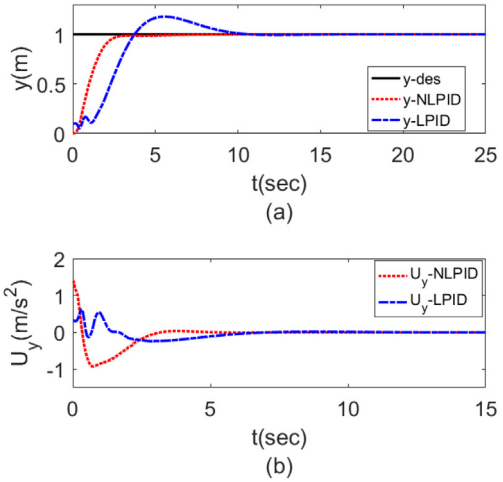

Fig. 6. y-Position (a) time response (b) controller signal.

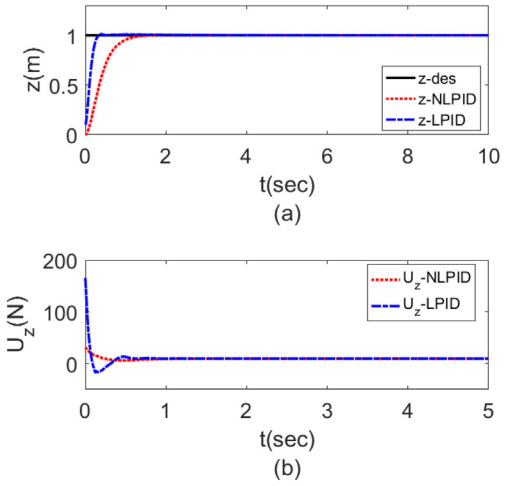

Fig. 7. z-Position (a) time response (b) controller signal.

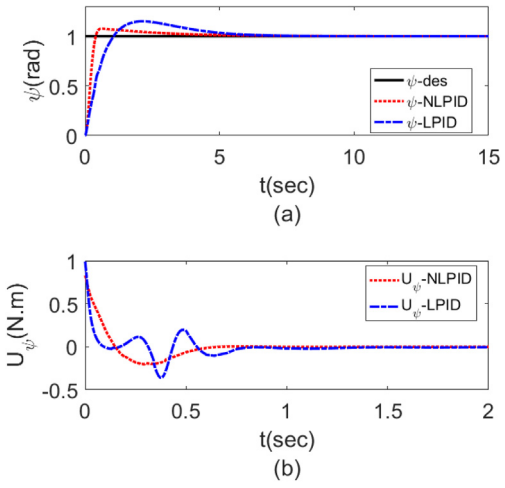

Fig. 8. ψ-Position (a) time response (b) controller signal.

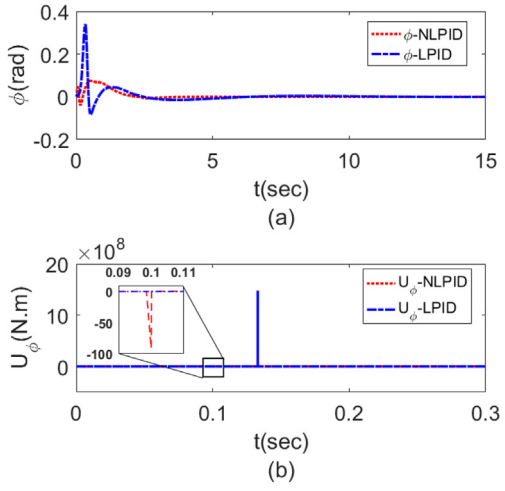

Fig. 9. ϕ-Position (a) time response (b) controller signal.

5.2. Trajectory tracking

In the following, the output responses of three case studies with trajectories generated by MATLAB/Simulink to test the overall 6-DOF UAV system using linear and nonlinear PID controllers will be presented and discussed. The cases studied have been chosen to reflect the difficulties that the quadcopter control system might face in achieving the required tracking. For all of the case studies, the initial values are $x = 0.1, y = 0.1, z = 0.1$ and the rest of the states are zero.

Case Study (1) The first test case study was the circular path. The states with the reference trajectories are presented in Table 9.

Fig. 11 shows the tracking of the 6-DOF UAV system for the circular trajectory. The proposed NLPID controller followed the trajectory with less time and smaller error than in the LPID one. The steady state error in the LPID controller was $e_x = 27\%, e_y = 18\%$, and $e_z = 0\%$, while in the proposed NLPID controller, the steady state error was $e_x = 0.56\%, e_y = 4.12\%$, and $e_z = 0\%$.

Case Study (2) The second test case was the helical path, in this case study the altitude z of the 6-DOF UAV is varying with time, in contrast to the first case study. The states with reference trajectories are presented in Table 10.

The LPID controller follows the desired trajectory with constant offset for the entire time of the simulations. While the proposed NLPID controller showed an improved performance over the LPID one as shown in Fig. 12.

Case Study (3) The final case study is the square trajectory. This trajectory is a serious test for the controllers designed for the UAV systems to accomplish the required track, since, the trajectory changes its direction suddenly at certain times (i.e., at the vertices of the square). The states with reference trajectories are presented in Table 11.

We can see the difference between the responses of both controllers in Fig. 13. The significance of the NLPID controller is very obvious, it tracked faster than the LPID one with very small overshoot as compared to the LPID controller. The overshoot in the LPID reached approximately up to 200% of the desired trajectory.

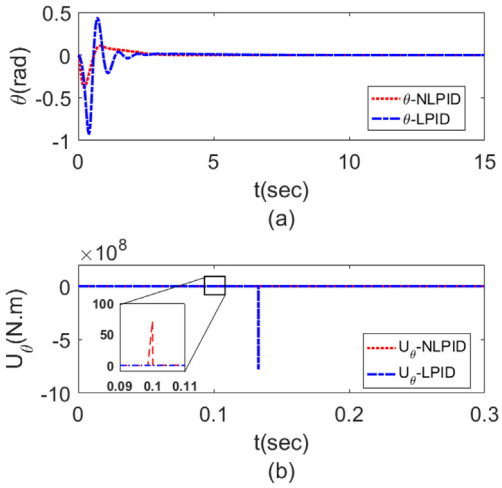

Fig. 10. θ-Position (a) time response (b) controller signal.

Table 7
Position and Yaw responses.

	LPID			NLPID		
	$t_r(s)$	$t_s(s)$	$M_p\%$	$t_r(s)$	$t_s(s)$	$M_p\%$
x	6.546	13.679	7.471	1.152	4.657	0.505
y	1.934	9.748	19.375	1.572	3.023	0.195
z	0.194	0.314	1.531	0.677	1.283	0.505
ψ	0.681	5.660	19.014	0.252	3.840	8.152

Table 8
Roll and Pitch responses.

	LPID		NLPID	
	Min peak	Max peak	Min peak	Max peak
θ	-8.292×10^{-2}	3.91×10^{-1}	-3.951×10^{-2}	7.402×10^{-2}
ψ	-9.195×10^{-1}	4.385×10^{-1}	-3.775×10^{-1}	1.065×10^{-1}

Table 9
Case 1 input signals.

State	Reference Trajectory	Time
x	$cos(0.1\pi t)$	$5 - t_f$
y	$sin(0.1\pi t)$	$5 - t_f$
z	$u(t)$	$0 - t_f$
ψ	$u(t)$	$0 - t_f$

*$t_f = 50$ s.

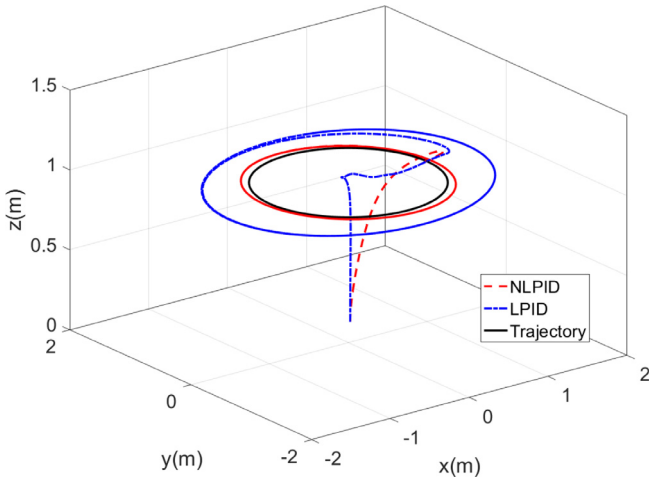

Fig. 11. Case 1 – Circular Trajectory.

5.3. Tracking with disturbances and measurements noise

In this section, we compare the performance of the proposed NLPID controller with that of the traditional PID one in the existence of exogenous disturbances and measurement noise. A step references are applied for the position and the heading of the quadrotor (x, y, z and ψ) while supposing that the quadrotor is facing a unity pulses wind disturbances which applied on the horizontal position (x, y) of the 6-DOF UAV quadrotor system (i.e. $f_{wx} = 1$ during $t = (25 - 27)$ s, $f_{wy} = 1$ during $t = (75 - 77)$ s). The results are shown in Fig. 14. From the results shown, it is obvious that the proposed NLPID attenuate the disturbances within a short period with small peak values in the output response. While the LPID react to the disturbances with a slower response and excessive over and/or undershoots in the output response. The reason behind this behavior is due to the fact that the gains of the LPID controller remain unchanged for all error values while the gains of the proposed NLPID are adjusted depending on the error values as mentioned previously in subsection 4.1.

Another important case study to validate the performance of the NLPID is the existence noise in the measured signals. We impose a different additive Gaussian noise with zero mean applied

Table 10
Case 2 input signals.

State	Reference Trajectory	Time
x	$cos(0.1\pi t)$	$5 - t_f$
y	$sin(0.1\pi t)$	$5 - t_f$
z	$0.2t$	$0 - t_f$
ψ	$u(t)$	$0 - t_f$

*$t_f = 100$ s.

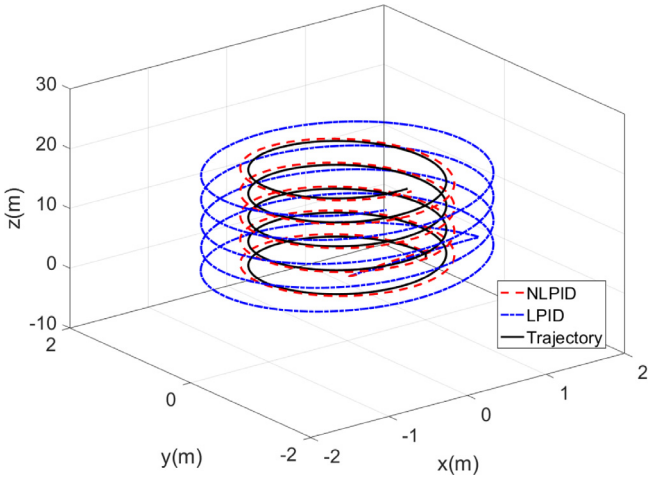

Fig. 12. Case 2 – Helical Trajectory.

Table 11
Case 3 input signals.

State	Reference Trajectory	Time
x	$u(t-10) - u(t-50)$	$10 - 50$
y	$u(t-30) - u(t-70)$	$30 - 70$
z	$u(t)$	$0 - t_f$
ψ	$u(t)$	$0 - t_f$

*$t_f = 100$ s.

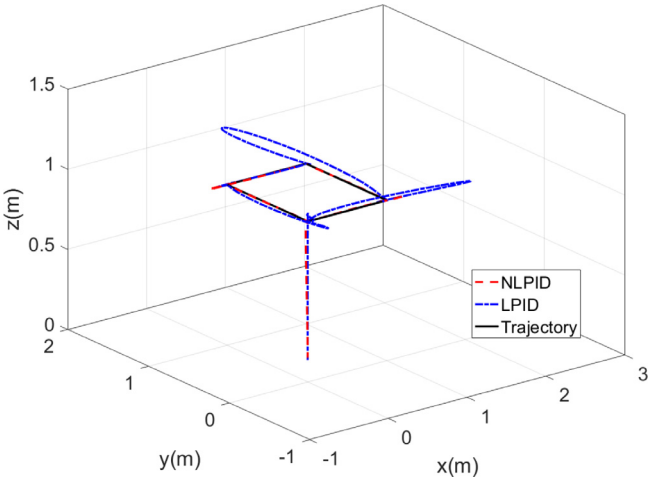

Fig. 13. Case 3 – Square Trajectory.

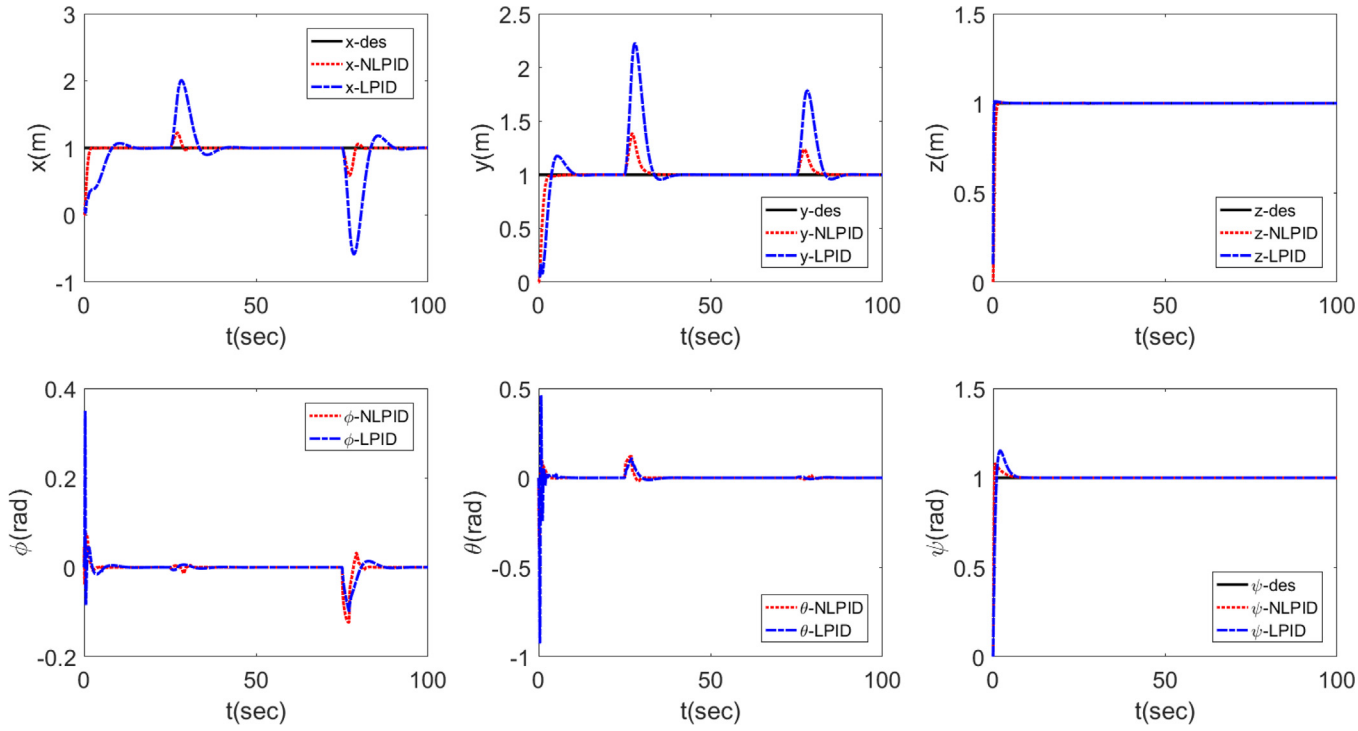

Fig. 14. Tracking with disturbances.

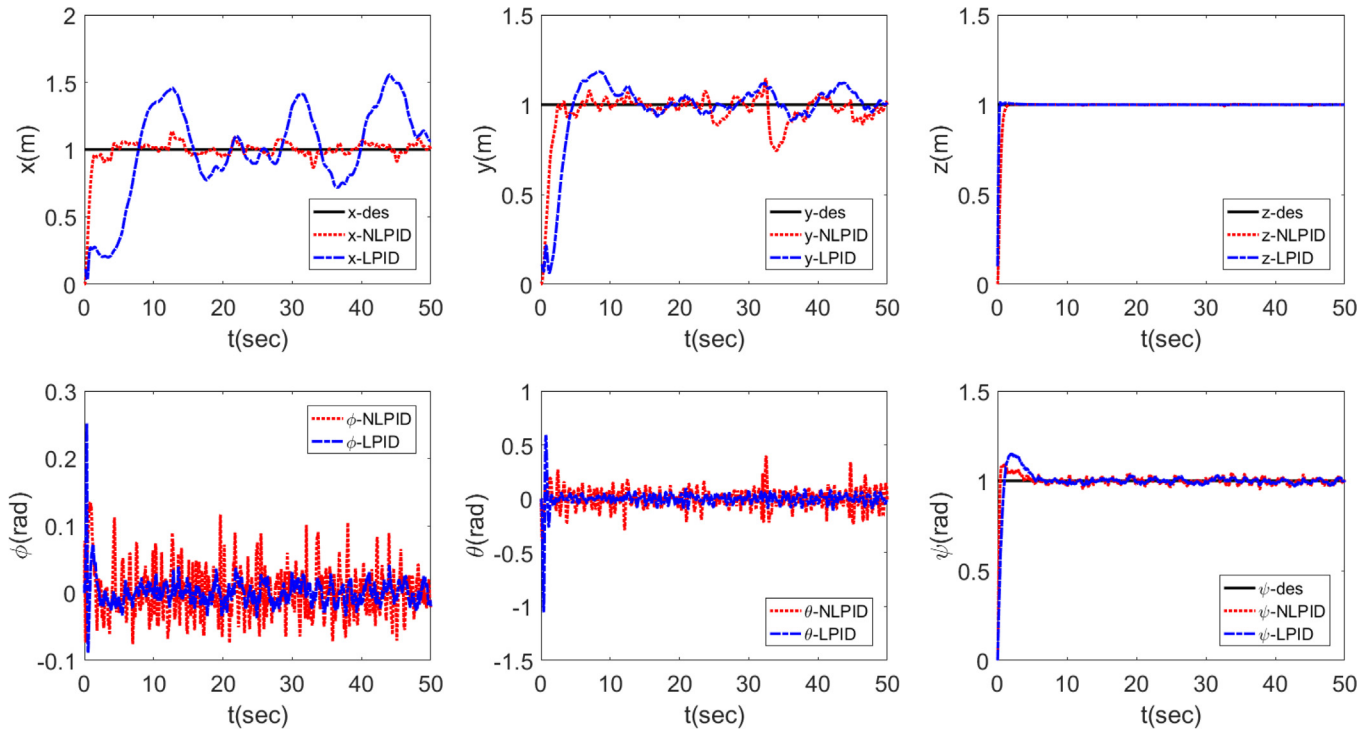

Fig. 15. Tracking with measurement noise.

for the different measured signals (10^{-8} variance for x and $y, 4 \times 10^{-8}$ variance for z and 10^{-2} variance for ϕ, θ and ψ). All the states results are shown in Fig. 15, where the responses of the signals (ϕ and θ) are worse with the NLPID controller, but this effects in a good performance and more robust behavior for the proposed NLPID controller than the LPID one for the position and the heading signals (x, y, z and ψ).

6. Conclusion and future work

In this work, the complete nonlinear model of the 6-DOF UAV was adopted with the aim of designing a NLPID controller for the stabilization and reference tracking for this complex, open-loop unstable, and highly nonlinear system. A new NLPID controller for stabilizing and controlling a 6-DOF UAV system is proposed

in this paper. The stability analysis for the closed-loop systems of both the position and orientation of the 6-DOF UAV system based on Hurwitz stability criterion was analyzed and proved that the proposed controller stabilized the system and accomplished the required tracking. From the simulation tests, it can be concluded that the proposed NLPID controller is better than the linear one in terms of speed, control energy, and steady-state error. In the near future work, we will study the performance of a real 6-DOF UAV quadrotor system using active disturbance rejection control paradigm to actively reject the wind disturbances and attenuate the effect of measurement noise.

Acknowledgment

A special thanks go to the Dr. Wameedh Riyadh Abdul-Adheem for the deep discussions on the topics of this paper.

References

[1] P.V. Kumar, A. Challa, J. Ashok, G.L. Narayanan, GIS based fire rescue system for industries using Quad copter – a novel approach, in: 2015 International Conference on Microwave, Optical and Communication Engineering (ICMOCE) IEEE, 2015, pp. 72–75, https://doi.org/10.1109/ICMOCE.2015.7489693.

[2] O.I. Dallal Bashi, W.Z. Wan Hasan, N. Azis, S. Shafie, H. Wagatsuma, Quadcopter sensing system for risky area, in: IEEE Regional Symposium on Micro and Nanoelectronics (RSM), 2017, IEEE, 2017, pp. 216–219, https://doi.org/10.1109/RSM.2017.8069152. URLhttp://ieeexplore.ieee.org/document/8069152/.

[3] H. Saha, S. Basu, S. Auddy, R. Dey, A. Nandy, D. Pal, N. Roy, S. Jasu, A. Saha, S. Chattopadhyay, T. Maity, A low cost fully autonomous GPS (Global Positioning System) based quad copter for disaster management, in: IEEE 8th Annual Computing and Communication Workshop and Conference (CCWC), 2018, IEEE, 2018, pp. 654–660, https://doi.org/10.1109/CCWC.2018.8301782. no. 0, http://ieeexplore.ieee.org/document/8301782/.

[4] J. Navia, I. Mondragon, D. Patino, J. Colorado, Multispectral mapping in agriculture: terrain mosaic using an autonomous quadcopter UAV, in: 2016 International Conference on Unmanned Aircraft Systems (ICUAS), IEEE, 2016, pp. 1351–1358, https://doi.org/10.1109/ICUAS.2016.7502606. URLhttp://ieeexplore.ieee.org/document/7502606/.

[5] R. Daroya, M. Ramos, NDVI image extraction of an agricultural land using an autonomous quadcopter with a filter-modified camera, in: 2017 7th IEEE International Conference on Control System, Computing and Engineering (ICCSCE), no. 0, IEEE, 2017, pp. 110–114.https://doi.org/10.1109/ICCSCE.2017.8284389.http://ieeexplore.ieee.org/document/8284389/.

[6] G. Hunt, F. Mitzalis, T. Alhinai, P.A. Hooper, M. Kovac, 3D printing with flying robots, in: 2014 IEEE International Conference on Robotics and Automation (ICRA), IEEE, 2014, pp. 4493–4499, https://doi.org/10.1109/ICRA.2014.6907515. URLhttp://ieeexplore.ieee.org/document/6907515/.

[7] E. Camci, E. Kayacan, Waitress quadcopter explores how to serve drinks by reinforcement learning, in: 2016 IEEE Region 10 Conference (TENCON), IEEE, 2016, pp. 28–32. doi:10.1109/TENCON.2016.7847952. http://ieeexplore.ieee.org/document/7847952/

[8] S.J. Kim, Y. Jeong, S. Park, K. Ryu, G. Oh, A survey of drone use for entertainment and AVR augmented and virtual reality, in: T. Jung, M.C. tom Dieck (Eds.), Augmented Reality and Virtual Reality, Progress in IS, Springer International Publishing, Cham, 2018, pp. 339–352, https://doi.org/10.1007/978-3-319-64027-3_23. URLhttp://link.springer.com/10.1007/978-3-319-64027-3_23.

[9] A. Eskandarpour, V.J. Majd, Cooperative formation control of quadrotors with obstacle avoidance and self collisions based on a hierarchical MPC approach, in: 2014 Second RSI/ISM International Conference on Robotics and Mechatronics (ICRoM), IEEE, 2014, pp. 351–356, https://doi.org/10.1109/ICRoM.2014.6990926. URLhttp://ieeexplore.ieee.org/document/6990926/.

[10] A. Rabah, W. Qing-he, Adaptive leader follower control for multiple quadrotors via multiple surfaces control, J. Beijing Inst. Technol. (English Edition) 25 (4) (2016) 526–532, https://doi.org/10.15918/j.jbit1004-0579.201625.0411. URLhttp://journal.bit.edu.cn/yw/bjlgyw/ch/reader/create_pdf.aspx?file_no=20160411&year_id=2016&quarter_id=4&falg=1.

[11] K.A. Ghamry, Y. Zhang, Cooperative control of multiple UAVs for forest fire monitoring and detection, in: 2016 12th IEEE/ASME International Conference on Mechatronic and Embedded Systems and Applications (MESA), IEEE, 2016, pp. 1–6, https://doi.org/10.1109/MESA.2016.7587184.

[12] Z. Hou, W. Wang, G. Zhang, C. Han, A survey on the formation control of multiple quadrotors, in: 2017 14th International Conference on Ubiquitous Robots and Ambient Intelligence (URAI), IEEE, 2017, pp. 219–225, https://doi.org/10.1109/URAI.2017.7992717.

[13] D. Kotarski, Z. Benic, M. Krznar, Control design for unmanned aerial vehicles with four rotors, Interdiscip. Description Complex Syst. 14 (2) (2016) 236–245, https://doi.org/10.7906/indecs.14.2.12. URLhttp://indecs.eu/index.php?s=x&y=2016&p=236-245.

[14] N. Hadi, A. Ramz, Tuning of PID controllers for quadcopter system using hybrid memory based gravitational search algorithm particle swarm optimization, Int. J. Comput. Appl. 172 (4) (2017) 9–18, https://doi.org/10.5120/ijca2017915125. URLhttp://www.ijcaonline.org/archives/volume172/number4/abbas-2017-ijca-915125.pdf.

[15] M. Akhil, M.K. Anand, A. Sreekumar, P. Hithesan, Simulation of the mathematical model of a quad rotor control system using matlab simulink, Appl. Mech. Mater. 110–116 (2011) 2577–2584, https://doi.org/10.4028/www.scientific.net/AMM.110-116.2577. URLhttp://www.scientific.net/AMM.110-116.2577.

[16] M.A. Alsharif, Y.E. Arslantas, M.S. Holzel, A comparison between advanced model-free PID and model-based LQI attitude control of a quadcopter using asynchronous android flight data, in: 2017 25th Mediterranean Conference on Control and Automation (MED), IEEE, 2017, pp. 1023–1028, https://doi.org/10.1109/MED.2017.7984252. URLhttp://ieeexplore.ieee.org/document/7984252/.

[17] I.K. Ibraheem, G.A. Ibraheem, Motion control of an autonomous mobile robot using modified particle swarm optimization based fractional order PID controller, Eng. Technol. J. 34 (13) (2016) 2406–2419.

[18] A. Kumar, A nonlinear fractional order PID controller applied to redundant robot manipulator, in: 2017 6th International Conference on Computer Applications In Electrical Engineering-Recent Advances (CERA), vol. 2018-Janua, IEEE, 2017, pp. 527–532.https://ieeexplore.ieee.org/document/8343385/.

[19] R. Lucas, R.M. Oliveira, C.B. Nascimento, M.S. Kaster, Performance analysis of an adaptive Gaussian nonlinear PID control applied to a step-down CC-CC converter, in: 2015 IEEE 24th International Symposium on Industrial Electronics (ISIE), Vol. 2015-Septe, IEEE, 2015, pp. 1022–1026, https://doi.org/10.1109/ISIE.2015.7281612. URLhttp://ieeexplore.ieee.org/document/7281612/.

[20] R.R. Benrezki, M. Tadjine, F. Yacef, O. Kermia, Passive fault tolerant control of quadrotor UAV using a nonlinear PID, in: 2015 IEEE International Conference on Robotics and Biomimetics (ROBIO), IEEE, 2015, pp. 1285–1290, https://doi.org/10.1109/ROBIO.2015.7418948.

[21] H. Li, Sliding-mode PID control of DC-DC converter, 2010 5th IEEE Conference on Industrial Electronics and Applications (2010) 730–734.https://doi.org/10.1109/ICIEA.2010.5516952.http://ieeexplore.ieee.org/lpdocs/epic03/wrapper.htm?arnumber=5516952.

[22] S. Gonzalez-Vazquez, J. Moreno-Valenzuela, A. New Nonlinear, PI, PID Controller for Quadrotor Posture Regulation, in IEEE Electronics, Robotics and Automotive Mechanics Conference, IEEE 2010 (2010) 642–647, https://doi.org/10.1109/CERMA.2010.78. URLhttp://ieeexplore.ieee.org/document/5692411/.

[23] Y. Bouzid, H. Siguerdidjane, Y. Bestaoui, Sliding modes based nonlinear PID controller for quadrotor – theory and experiment, Proceedings of the 14th International Conference on Informatics in Control, Automation and Robotics, vol. 1, SCITEPRESS – Science and Technology Publications, 2017, pp. 286–294, https://doi.org/10.5220/0006433402860294.

[24] L.M. Argentim, W.C. Rezende, P.E. Santos, R.A. Aguiar, PID LQR and LQR-PID on a quadcopter platform, in: 2013 International Conference on Informatics, Electronics and Vision (ICIEV), IEEE, 2013, pp. 1–6, https://doi.org/10.1109/ICIEV.2013.6572698.

[25] T. Lee, M. Leok, N.H. McClamroch, in: 49th IEEE Conference on Decision and Control (CDC), 2010, pp. 5420–5425, https://doi.org/10.1109/CDC.2010.5717652.

[26] P. Ru, K. Subbarao, Nonlinear model predictive control for unmanned aerial vehicles, Aerospace 4 (2) (2017) 1–26, https://doi.org/10.3390/aerospace4020031. URLhttp://www.mdpi.com/2226-4310/4/2/31.

[27] K.M. Thu, A. Gavrilov, Designing and modeling of quadcopter control system using L1 adaptive control, Proc. Comput. Sci. 103 (October 2016) (2017) 528–535, https://doi.org/10.1016/j.procs.2017.01.046. URLhttp://linkinghub.elsevier.com/retrieve/pii/S1877050917300479.

[28] E.A. Seidabad, S. Vandaki, A.V. Kamyad, Designing fuzzy PID controller for quadrotor, Int. J. Adv. Res. Comput. Sci. Technol. (IJARCST 2014 2 (4) (2014) 221–227. URLhttp://www.ijarcst.com/doc/vol2-issue4/ver.2/saeed_vandaki.pdf.

[29] Eduardo M. Bucio-Gallardo, Ricardo Zavala-Yoé, Ricardo A. Ramírez-Mendoza, Mathematical model and intelligent control of a quadcopter, with non-conventional membership functions, J. Energy Power Eng. 10 (10) (2016) 634–642, https://doi.org/10.17265/1934-8975/2016.10.008. URLhttp://www.davidpublisher.org/index.php/Home/Article/index?id=28292.html.

[30] A. Zulu, S. John, A review of control algorithms for autonomous quadrotors, O. J. Appl. Sci. 04 (14) (2014) 547–556, https://doi.org/10.4236/ojapps.2014.414053.

[31] W.R. Abdul-Adheem, I.K. Ibraheem, From PID to nonlinear state error feedback controller, Int. J. Adv. Comput. Sci. Appl. 8 (1) (2017) 312–322, https://doi.org/10.14569/IJACSA.2017.080140. URLhttp://thesai.org/Publications/ViewPaper?Volume=8&Issue=1&Code=ijacsa&SerialNo=40.

[32] A.T. Nugraha, T. Agustinah, Quadcopter path following control design using output feedback with command generator tracker based on LOS, International Seminar on Intelligent Technology and Its Applications (ISITIA), vol. 947, IEEE, 2017, pp. 255–260, https://doi.org/10.1109/ISITIA.2017.8124090. URLhttp://ieeexplore.ieee.org/document/8124090/.

[33] F. Sabatino, Quadrotor control: modeling, nonlinear control design, and simulation, Master's thesis, Royal Institute of Technology (2015). https://www.kth.se/polopoly_fs/1.588039!/Thesis KTH - Francesco Sabatino.pdf.

[34] R.W. Beard, Quadrotor Dynamics and Control, Brigham Young University (June), 2008, pp. 1–47.
[35] I.K. Ibraheem, On the design of a novel finite-time nonlinear extended state observer for class of nonlinear systems with mismatch disturbances and uncertainties (2018) 1–36. arXiv:1805.00257.
[36] W.R. Abdul-Adheem, I.K. Ibraheem, Improved sliding mode nonlinear extended state observer based active disturbance rejection control for uncertain systems with unknown total disturbance, Int. J. Adv. Comput. Sci. Appl. 7 (12) (2016) 80–93, https://doi.org/10.14569/IJACSA.2016.071211. URLhttp://thesai.org/Publications/ViewPaper?Volume=7&Issue=12&Code=ijacsa&SerialNo=11.
[37] Tengfei Liu, Cong Wang, Learning from neural control of general Brunovsky systems, in: 2006 IEEE Conference on Computer Aided Control System Design, 2006 IEEE International Conference on Control Applications, 2006 IEEE International Symposium on Intelligent Control, Vol. 17, IEEE, 2006, pp. 2366–2371. doi:10.1109/CACSD-CCA-ISIC.2006.4777010. http://ieeexplore.ieee.org/document/4777010/.